inorganics

MDPI

Article

Two-Dimensional and Three-Dimensional Coordination Polymers Based on Ln(III) and 2,5-Diiodoterephthalates: Structures and Luminescent Behavior

Alexander S. Zaguzin [1,2], Mikhail A. Bondarenko [1,2], Pavel A. Abramov [1], Marianna I. Rakhmanova [1], Maxim N. Sokolov [1], Vladimir P. Fedin [1] and Sergey A. Adonin [1,2,*]

[1] Nikolaev Institute of Inorganic Chemistry SB RAS, Lavrentiev St. 3, 630090 Novosibirsk, Russia
[2] South Ural State University, Lelina St. 76, 454080 Chelyabinsk, Russia
* Correspondence: adonin@niic.nsc.ru

Abstract: Five new coordination polymers based on Ln^{3+} and 2,5-diiodoterephthalates (2,5-I-bdc)—{[La_2(2,5-I-bdc)$_3$(DMF)$_4$]}·2DMF (**1**) and {[Ln_2(2,5-I-bdc)$_3$(DMF)$_4$]} (Ln = La (**2**), Nd (**3**), Sm (**4**) and Eu (**5**))—were prepared and characterized by single crystal and powder X-ray diffractometry. Luminescent behavior was examined (the highest quantum yield is 4.5%); thermal stability was examined using thermogravimetric analysis.

Keywords: lanthanides; carboxylates; coordination polymers; iodinated arenes; crystal structure

check for updates

Citation: Zaguzin, A.S.; Bondarenko, M.A.; Abramov, P.A.; Rakhmanova, M.I.; Sokolov, M.N.; Fedin, V.P.; Adonin, S.A. Two-Dimensional and Three-Dimensional Coordination Polymers Based on Ln(III) and 2,5-Diiodoterephthalates: Structures and Luminescent Behavior. *Inorganics* **2022**, *10*, 262. https://doi.org/10.3390/inorganics10120262

Academic Editor: Valentina Utochnikova

Received: 24 November 2022
Accepted: 13 December 2022
Published: 16 December 2022

Publisher's Note: MDPI stays neutral with regard to jurisdictional claims in published maps and institutional affiliations.

Copyright: © 2022 by the authors. Licensee MDPI, Basel, Switzerland. This article is an open access article distributed under the terms and conditions of the Creative Commons Attribution (CC BY) license (https://creativecommons.org/licenses/by/4.0/).

1. Introduction

Metal-organic frameworks (MOFs) represent a large and rapidly growing class of compounds which have remained a focus of attention of chemists around the world in recent decades [1–3]. The interest in MOFs is driven by the fact that they can be utilized in numerous application areas, such as catalysis [4–6], the deep separation of diverse organic substrates, including hydrocarbons, [7–10] the design of selective sensors [11–15], etc. It is very important that the selectivity of these processes is governed predominantly by the nature of the organic linker ligands connecting the metal centers, since those are mostly responsible for the system of non-covalent interactions with the substrates.

Usually, the main role is played by hydrogen bonds (this is expected due to the greater number of C-H fragments in most organic ligands). However, other non-covalent interactions can participate in the binding of substrates as well. Among them, there is the halogen bond (XB), a type of supramolecular contact which has been intensively investigated within the last decade [16–22]. In some the recent works, it was shown that the XB can play a decisive role in the appearance of certain properties of MOFs [13,23,24]. For this reason, we believe that this area has a great potential for further development.

Within our current research, we focused on the use of iodine-substituted aromatic polycarboxylic acids as linkers for MOFs. This class of compounds has several important advantages. Earlier, it was shown [25] that they can indeed form rather strong halogen bonds. On the other hand, they can be regarded as very suitable linkers—there are hundreds, if not thousands, of MOFs based on derivatives of terephthalic, isophthalic, biphenyldicarboxylic and other acids.

The results of our work with 2-iodoterephthalic acid (2-I-bdc) revealed that MOFs based thereupon feature sorption selectivity strikingly different from one demonstrated by MOFs based on non-substituted bdc [26]. In further experiments, we decided to focus on a more iodine-rich bdc derivative, 2,5-diiodoterephthalic acid (2,5-I-bdc), and on lanthanides as metal centers in order to examine the luminescent properties of the resulting MOFs. Here, we report five novel Ln^{3+}-based MOFs—{[La_2(2,5-I-bdc)(DMF)$_4$}]·2DMF (**1**) and {[Ln_2(2,5-I-bdc)(DMF)$_4$}] (Ln = La (**2**), Nd (**3**), Sm (**4**) and Eu (**5**))—and discuss their structures and luminescent properties.

2. Materials and Methods

All reagents were obtained from commercial sources and used as purchased. H_2(2,5-I-bdc) was prepared according to the method described in the literature [27].

2.1. Synthesis of 1–5

20 mg (0.056 mmol) of $LnCl_3 \cdot 6H_2O$ (Ln = La (**1** and **2**), Nd (**3**), Sm (**4**) and Eu (**5**)), 35 mg (0.084 mmol) of H_2(2,5-I-bdc) and 7 mL of DMF were placed into a glass ampoule, which was sealed, treated in an ultrasonic bath (10 min) and kept at 120 °C for 48 h with slow cooling, resulting in the formation of crystals (mixture of **1** and **2**/**3**/**4**/**5**, respectively). The yields were: 89% (total for 1 and 2), 87% (**3**), 85% (**4**), and 91% (**5**). The data of element analysis are given in Supporting Information.

2.2. X-ray Diffractometry

Crystallographic data and refinement details for **1** and **2** are given in Table S1 (Supporting Information). The diffraction data were collected: (a) for **1**, on a Rigaku XtaLAB Synergy-S (Agilent Technologies) diffractometer with CuKα radiation (λ = 1.54184) by conducting φ scans of narrow (0.5°) frames at 100 K. Absorption correction was completed empirically using SCALE3 ABSPACK, and (b) for **2**, on a Bruker D8 Venture diffractometer with a CMOS PHOTON III detector and IμS 3.0 source (Mo Kα radiation, λ = 0.71073 Å) at 150 K. The φ- and ω-scan techniques were employed. Absorption correction was applied using SADABS (Bruker Apex3 software suite: Apex3, SADABS-2016/2 and SAINT, version 2018.7-2; Bruker AXS Inc.: Madison, WI, 2017). Structures were solved by SHELXT [28] and refined by full-matrix least-squares treatment against $|F|^2$ in anisotropic approximation with SHELX 2014/7 [29] in the ShelXle program. [30] H-atoms were refined in geometrically calculated positions. The main geometrical parameters are summarized in Table S2 (SI).

The disordering of DMF molecules over two closed positions in the crystal structure of **1** is a cause for the refinement of all participating atoms in isotropic approximation. In the case of **1** and **2,** there is some residual electronic density around I-atoms without any chemical sense, reflecting A- and B-type alerts during PLATON checks. In all cases, the residual electronic density does not exceed 10% over the electronic count of I.

The crystallographic data have been deposited in the Cambridge Crystallographic Data Centre under the deposition codes CCDC 2217191-2217192.

2.3. Powder X-ray Diffractometry

XRD analysis of polycrystals was performed on a Shimadzu XRD-7000 diffractometer (CuK-alpha radiation, Ni–filter, linear One Sight detector, 0.0143° 2θ step, 2s per step). The plotting of PXRD patterns and data treatment was performed using X'Pert Plus software (see Supporting Information).

2.4. Luminescence Measurements and Thermogravimetric Analysis (TGA)

See Supporting Information.

3. Results and Discussion

For the preparation of **1–5**, we used the solvothermal approach, which is widely applied in MOF chemistry [31–36]. The crystals of **1** and **2** were isolated from the same sample; as follows from the PXRD data (see Supporting Information), it contains **1, 2** and some other unidentified phase. The data of the element analysis agree well with the composition corresponding to **1** and **2**, so it can be assumed that the by-product has a similar composition. MOFs **3–5** were isolated as single phases.

It must be noted that all crystals in the **1–5** series were initially isolated in experiments where different N-linkers (such as 1,2-bis(4-pyridyl)ethane, 1,2-bis(4-pyridyl)ethylene and 4,4′-bipyridine) were added to the mixture. We aimed for the preparation of heteroleptic MOFs but this strategy did not work, clearly due to higher oxophilicity of Ln.

The main difference between **1** and isostructural series **2–5** is the absence/presence of solvate DMF molecules. In the crystal structure of **1,** binuclear $[La_2(C_6H_2I_2(COO)_2)_6(DMF)_4]$ building blocks (Figure 1; main bond distances are summarized in Table S2 of the supporting Information) combine into layers via bridging with dicarboxylate ligands. Such layers are oriented in the [110] crystal direction and stack together in an AAA . . . motif along the [001] crystal direction. Solvate DMF molecules fill the space between the layers. All $[La_2(C_6H_2I_2(COO)_2)_6(DMF)_4]$ dimeric units are symmetrically equal. Carboxylate ligands of the dimer connect each building block with its four neighbors (Figures 2 and 3).

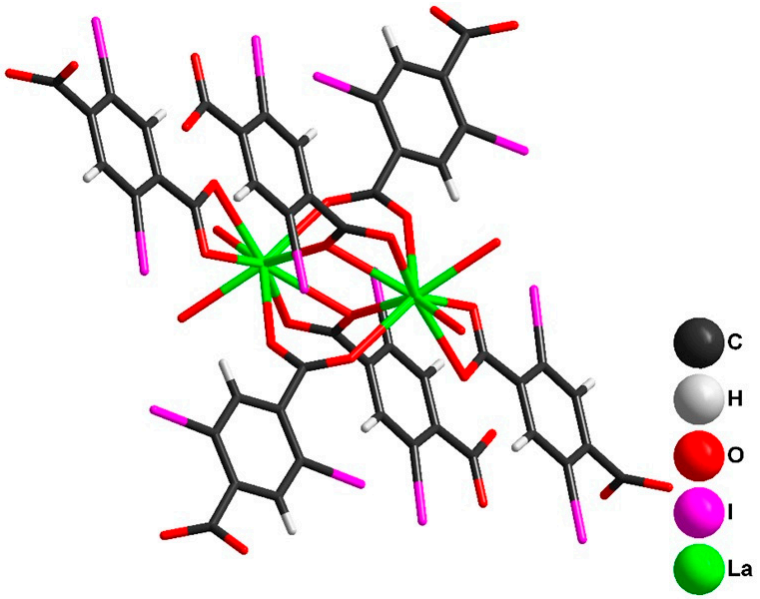

Figure 1. Structure of $[La_2(2,5\text{-I-bdc})_6(DMF)_4]$ in the crystal structure of **1**. Disordered DMF molecules are omitted for clarity (only O-atoms are shown).

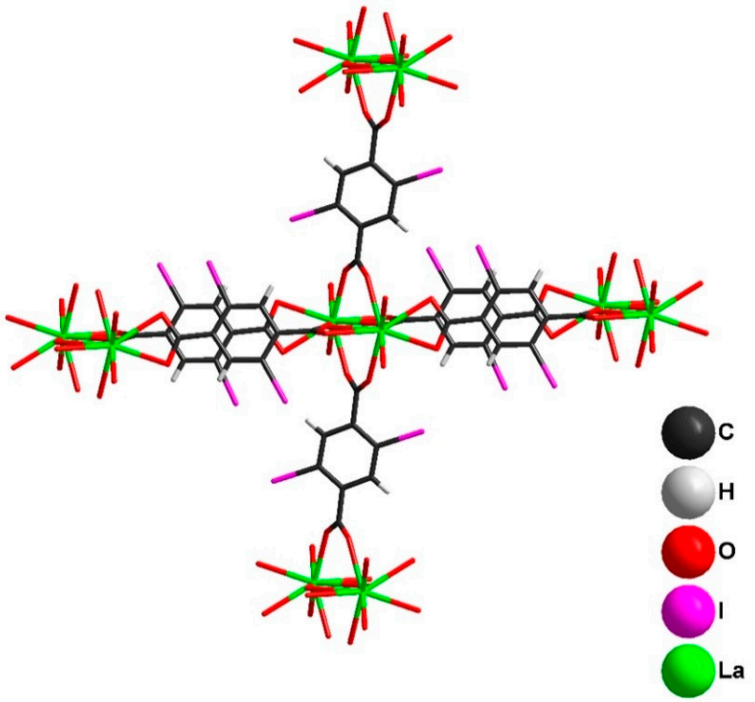

Figure 2. Connectivity between $[La_2(2,5\text{-I-bdc})_6(DMF)_4]$ units in the crystal structure of **1**. Disordered DMF molecules are omitted for clarity (only O-atoms shown).

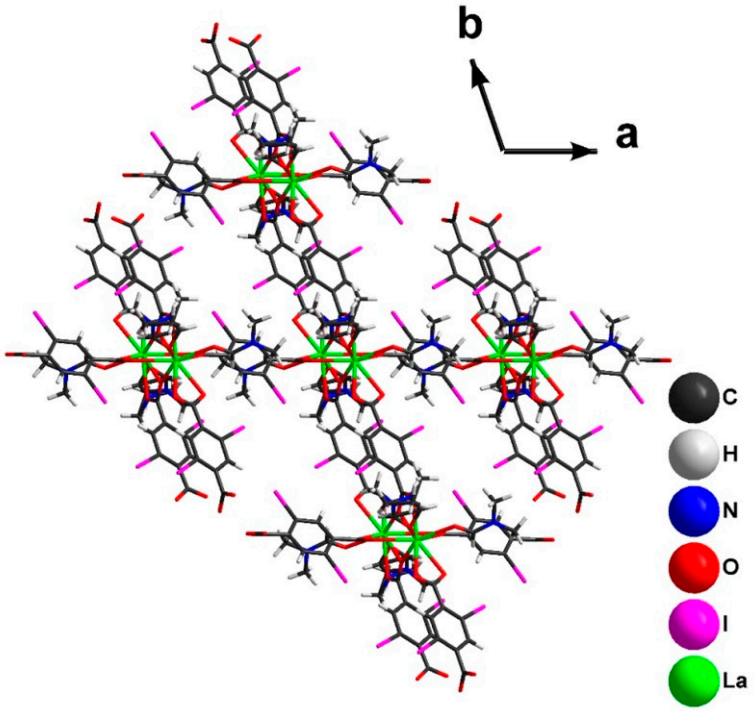

Figure 3. Layers formed by $[La_2(2,5\text{-I-bdc})_6(DMF)_4]$ units in the crystal structure of **1**.

In the crystal structure of **2,** the binuclear geometry of $[La_2(2,5\text{-I-bdc})_6(DMF)_4]$ binuclear units is significantly different due to the absence of solvate DMF molecules. A comparison of the geometry of such dimers in the crystal structures of **1** and **2** is presented in Figure 4.

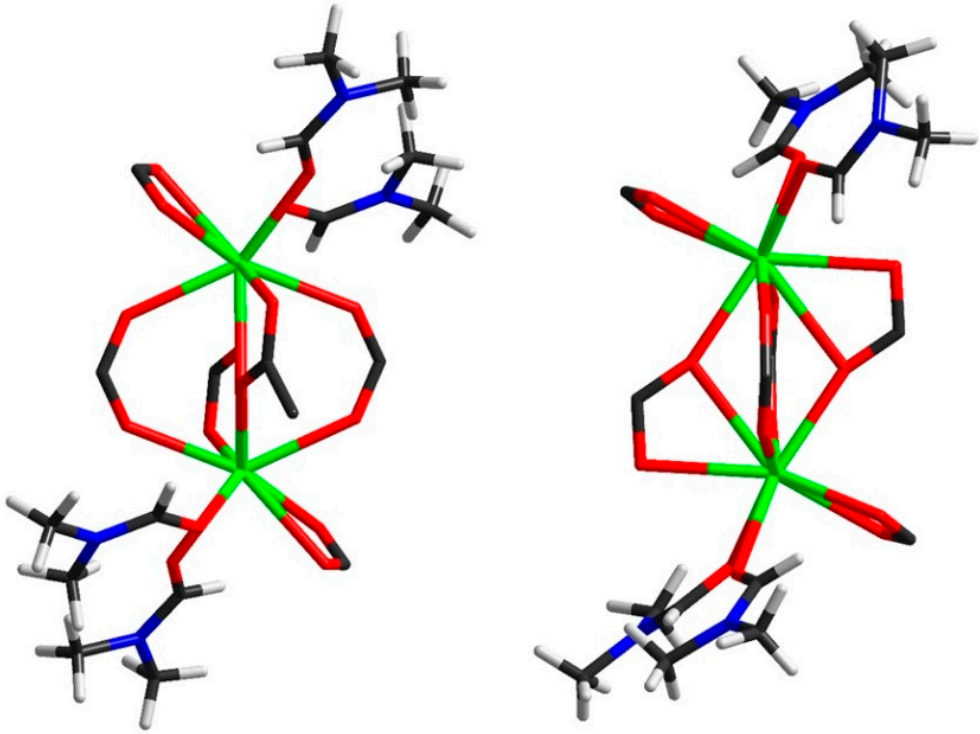

Figure 4. Geometry of the $[La_2(2,5\text{-I-bdc})_6(DMF)_4]$ units in **1** (**left**) and **2** (**right**).

The reorientation of dicarboxylic ligands (Figure 5) leads to a change in the topology of the coordination polymer from 2D to 3D. In the crystal structure of **2**, each dimer

is connected with six neighboring ones (Figure 6). The crystal packing of **2** (Figure 7) demonstrates the presence of 1D channels in the [001] crystal direction. These channels are decorated by I-atoms potentially accessible for non-covalent interactions with different substrates.

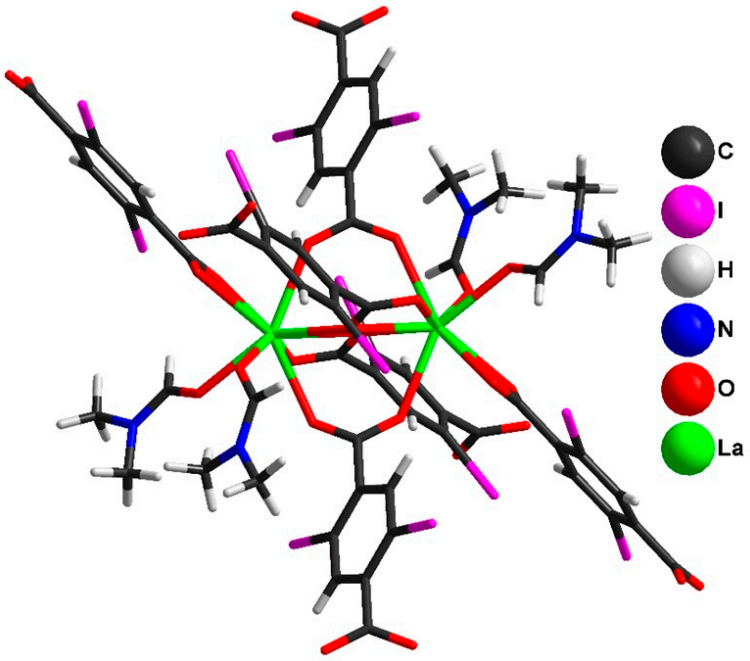

Figure 5. Structure of $[La_2(2,5\text{-I-bdc})_6(DMF)_4]$ in the crystal structure of **2**.

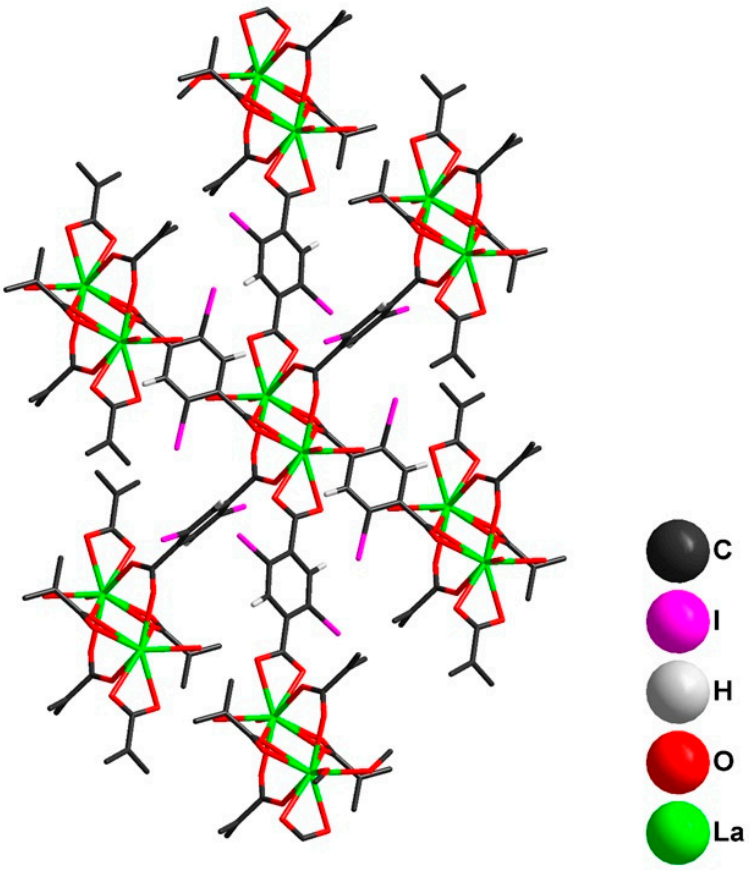

Figure 6. Connectivity between $[La_2(2,5\text{-I-bdc})_6(DMF)_4]$ units in the crystal structure of **2**.

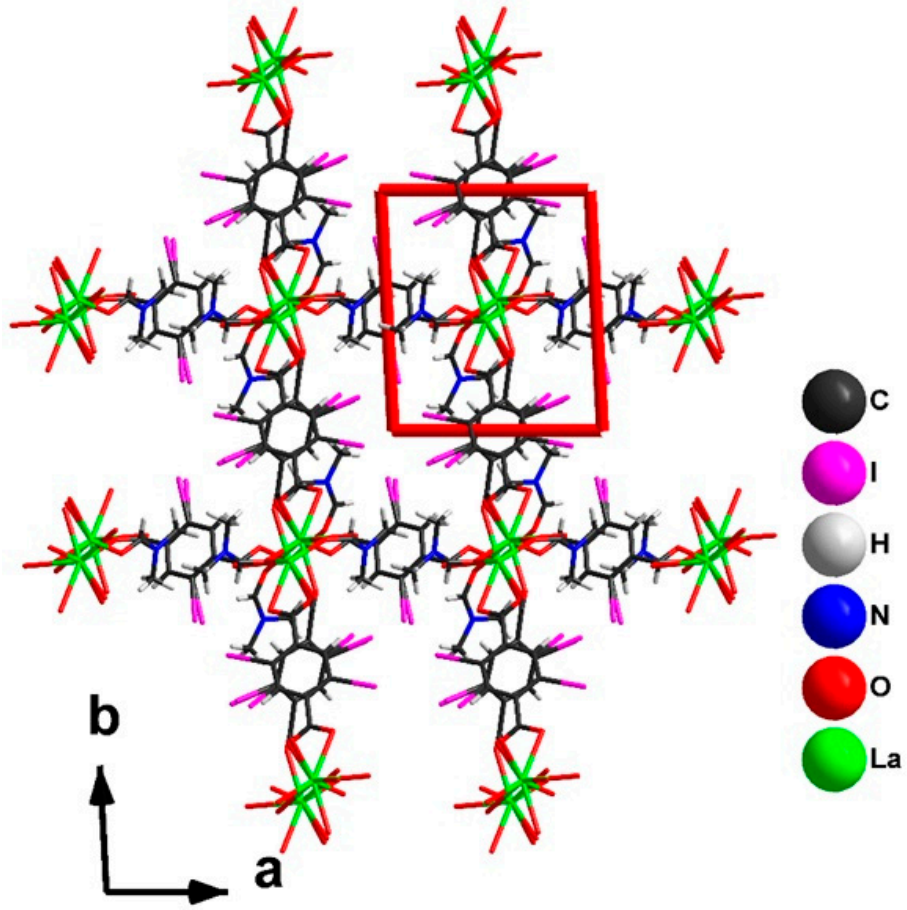

Figure 7. Crystal packing of **2**.

Luminescence of Ln^{3+} carboxylate complexes has been widely studied in recent years [37–42], so we decided to study these features for the **1**/**2** mixture as well as the pure **3**, **4** and **5** phases. The excitation and emission spectra of the complexes (λ_{ex} = 340 nm) are shown in Figure 8 (see also Figures 9 and 10 for details). The emission spectra of the solid containing **1** and **2** exhibits only the band at 445 nm. Because La^{3+} is a non-luminescent ion, these spectra show the optical properties of the ligand luminescence [43]. The measured lifetime of the luminescence is τ = 5 ns. The blue emission has the colorimetric coordinates (0.150, 0.128).

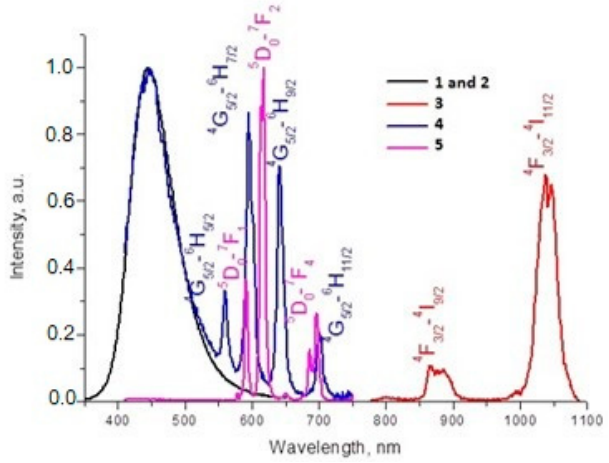

Figure 8. Emission spectra of complexes after excitation at 340 nm.

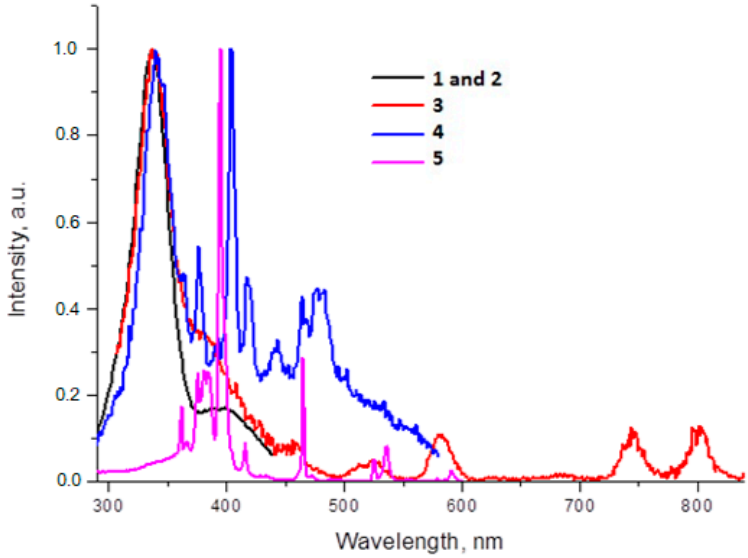

Figure 9. Excitation spectra of complexes registered for most intensive emission line ((1/2)-λem = 445 nm, (3)-λem = 1060 nm, (4)-λem = 601 nm, (5)-λem = 615 nm).

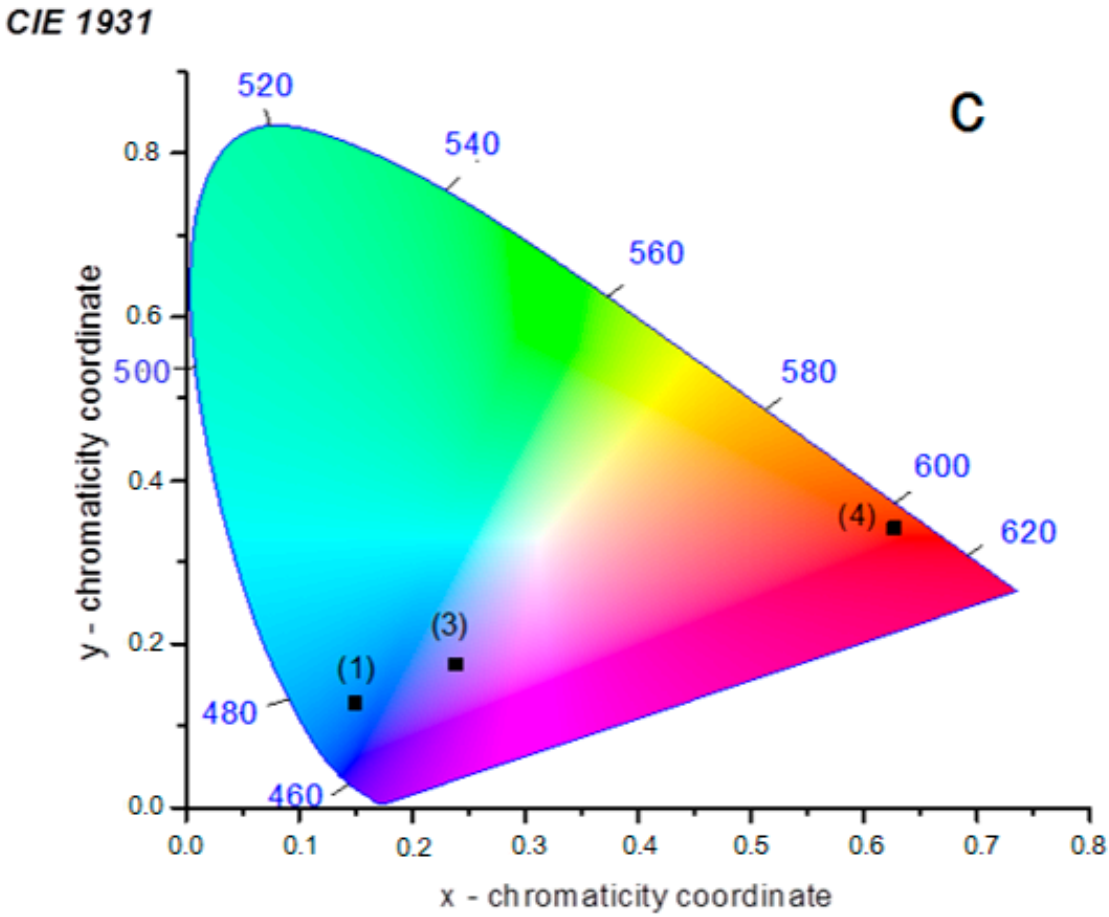

Figure 10. CIE chromaticity diagram for (**1**/**2**) (x = 0.150, y = 0.128), (**4**) (x = 0.238, y = 0.175), (**5**) (x = 0.627, y = 0.342).

The photoluminescence spectra of the (**3**) complex have pronounced peaks corresponding to $^4F^{3/2} \rightarrow {}^4I_{9/2}$ (880 nm) and $^4F^{3/2} \rightarrow {}^4I_{11/2}$ (1060 nm) transitions in Nd^{3+}. The most intensive emission band observed at 1060 nm corresponds to the $^4F^{3/2} \rightarrow {}^4I_{11/2}$ transition. The excitation spectra obtained by monitoring the luminescence at λ = 1060 nm showed

some narrow excitation bands (λ = 500–850 nm region) and a large band (λ < 400 nm), which were attributed to the absorption of the Nd^{3+} central ion and ligand moieties, respectively. The luminescence spectrum of compound (**4**) in the visible region exhibited the characteristic emission bands for Sm^{3+} ($^4G_{5/2} \rightarrow {}^6H_{5/2}$, $^4G_{5/2} \rightarrow {}^6H_{7/2}$, $^4G_{5/2} \rightarrow {}^6H_{9/2}$ and $^4G_{5/2} \rightarrow {}^6H_{11/2}$). The most intense emission line corresponded to the hypertensive $^4G_{5/2} \rightarrow {}^6H_{7/2}$ (601 nm) transition and a ligand-centered emission at 445 nm induces a purple light emission with the colorimetric coordinates (0.238, 0.175). The luminescent lifetime for complex (**4**) is 50 μs and the quantum yield is < 1%. The excitation spectrum of (**4**) has a broad band in the region of 290–370 nm, which is ascribed to the π–π* electronic transition of the ligand, and narrow bands in the region of 400–500 nm, which are attributed to the intraconfigurational $f-f$ transitions of the Sm^{3+} ion.

For compound (**5**), the following transitions are observed: $^5D_0 \rightarrow {}^7F_1$, $^5D_0 \rightarrow {}^7F_2$, $^5D_0 \rightarrow {}^7F_3$, and $^5D_0 \rightarrow {}^7F_4$. The intensity of the emission of the forced electric dipole transition of Eu^{3+} $^5D_0 \rightarrow {}^7F_2$ (615 nm) of compound (**5**) dominated the spectrum. The rest of the emission bands were small compared with the latter. It has been previously reported that these characteristics are indicative of low-symmetry Eu^{3+} coordination compounds [44]. Additionally, the emission peak centered at 615 nm is the strongest one, which results in a red emission with the colorimetric coordinates (0.627, 0.342). The luminescent lifetime for complex (**5**) is 1.1 ms and the quantum yield is 4.5%. The excitation spectrum of (**3**) contains a broad band ranging from 290 to 360 nm, which is ascribed to the π–π* electronic transition of the ligand. The narrow bands in the region of 360–600 nm are attributed to the intraconfigurational f−f transitions of the Eu^{3+} ion.

TGA data for **4** and **5** are given in SI (Figure S5 and Figure S6, respectively). Those are almost identical: there is a clear stage of DMF elimination (≈16% of total mass) occurring within the T range up to ≈120 °C.

4. Conclusions

To conclude, we demonstrated that 2,5-diiodoterephthalate is an efficient linker for the design of lanthanide-based MOFs. However, in the absence of auxiliary O-containing linkers, additional coordination sites are occupied by DMF molecules so that they can form either 2D or 3D polymers. Most likely, this series can be expanded to other Ln^{3+} -based MOFs, potentially resulting in complexes with greater emission properties. Corresponding experiments are underway.

Supplementary Materials: The following supporting information can be downloaded at: https://www.mdpi.com/article/10.3390/inorganics10120262/s1. XRD, PXRD, luminescence and TGA details.

Author Contributions: Conceptualization, S.A.A.; methodology, S.A.A. and V.P.F.; validation, A.S.Z. and M.N.S., formal analysis, S.A.A., M.I.R. and V.P.F.; investigation, M.A.B., A.S.Z., P.A.A. and M.I.R.; resources, S.A.A.; data curation, M.A.B. and P.A.A.; writing—original draft preparation, S.A.A., P.A.A. and M.I.R.; writing—review and editing, M.N.S.; visualization, M.I.R. and S.A.A.; supervision, S.A.A.; project administration, S.A.A.; funding acquisition, S.A.A. All authors have read and agreed to the published version of the manuscript.

Funding: This research was supported by the Russian Science Foundation (Grant No. 21-73-20019) and, in part, by the Ministry of Science and Higher Education of the Russian Federation (121031700313-8, spectral characterization).

Institutional Review Board Statement: Not applicable.

Informed Consent Statement: Not applicable.

Data Availability Statement: Not applicable.

Acknowledgments: The authors thank the Resource center of Saint Petersburg State University for assistance in the XRD experiments and Pavel E. Plyusnin (NIIC SB RAS) for assistance with the TGA experiments.

Conflicts of Interest: The authors declare no conflict of interest.

References

1. Cohen, S.M. Postsynthetic methods for the functionalization of metal-organic frameworks. *Chem. Rev.* **2012**, *112*, 970–1000. [CrossRef] [PubMed]
2. Adegoke, K.A.; Maxakato, N.W. Porous metal-organic framework (MOF)-based and MOF-derived electrocatalytic materials for energy conversion. *Mater. Today Energy* **2021**, *21*, 970–1000. [CrossRef]
3. Gorbunova, Y.G.; Fedin, V.P.; Blatov, V.A. Metal-organic frameworks as the basis for new-generation functional materials. *Russ. Chem. Rev.* **2022**, *91*, 100816. [CrossRef]
4. Liu, Y.; Xuan, W.; Cui, Y. Engineering homochiral metal-organic frameworks for heterogeneous asymmetric catalysis and enantioselective separation. *Adv. Mater.* **2010**, *22*, 4112–4135. [CrossRef] [PubMed]
5. Mulik, N.; Bokade, V. Immobilization of HPW on UiO-66-NH_2 MOF as efficient catalyst for synthesis of furfuryl ether and alkyl levulinate as biofuel. *Mol. Catal.* **2022**, *531*, 112689. [CrossRef]
6. Isaeva, V.I.; Nefedov, O.M.; Kustov, L.M. Metal–Organic Frameworks-Based Catalysts for Biomass Processing. *Catalysts* **2018**, *8*, 368. [CrossRef]
7. Sapianik, A.A.; Dudko, E.R.; Kovalenko, K.A.; Barsukova, M.O.; Samsonenko, D.G.; Dybtsev, D.N.; Fedin, V.P. Metal-Organic Frameworks for Highly Selective Separation of Xylene Isomers and Single-Crystal X-ray Study of Aromatic Guest-Host Inclusion Compounds. *ACS Appl. Mater. Interfaces* **2021**, *13*, 14768–14777. [CrossRef]
8. Sapchenko, S.A.; Dybtsev, D.N.; Samsonenko, D.G.; Belosludov, R.V.; Belosludov, V.R.; Kawazoe, Y.; Schröder, M.; Fedin, V.P. Selective gas adsorption in microporous metal-organic frameworks incorporating urotropine basic sites: An experimental and theoretical study. *Chem. Commun.* **2015**, *51*, 13918–13921. [CrossRef]
9. Han, X.; Yang, S.; Schröder, M. Porous metal–organic frameworks as emerging sorbents for clean air. *Nat. Rev. Chem.* **2019**, *3*, 108–118. [CrossRef]
10. Trenholme, W.J.F.; Kolokolov, D.I.; Bound, M.; Argent, S.P.; Gould, J.A.; Li, J.; Barnett, S.A.; Blake, A.J.; Stepanov, A.G.; Besley, E.; et al. Selective Gas Uptake and Rotational Dynamics in a (3,24)-Connected Metal-Organic Framework Material. *J. Am. Chem. Soc.* **2021**, *143*, 3348–3358. [CrossRef]
11. Kreno, L.E.; Leong, K.; Farha, O.K.; Allendorf, M.; Van Duyne, R.P.; Hupp, J.T. Metal-organic framework materials as chemical sensors. *Chem. Rev.* **2012**, *112*, 1105–1125. [CrossRef] [PubMed]
12. Zhang, Y.; Yuan, S.; Day, G.; Wang, X.; Yang, X.; Zhou, H.-C. Luminescent sensors based on metal-organic frameworks. *Coord. Chem. Rev.* **2018**, *354*, 28–45. [CrossRef]
13. Norouzi, F.; Khavasi, H.R. Iodine decorated-UiO-67 MOF as a fluorescent sensor for the detection of halogenated aromatic hydrocarbons. *New J. Chem.* **2020**, *44*, 8937–8943. [CrossRef]
14. Yang, Z.; Zhang, W.; Yin, Y.; Fang, W.; Xue, H. Metal-organic framework-based sensors for the detection of toxins and foodborne pathogens. *Food Control* **2022**, *133*, 108684. [CrossRef]
15. Small, L.J.; Hill, R.C.; Krumhansl, J.L.; Schindelholz, M.E.; Chen, Z.; Chapman, K.W.; Zhang, X.; Yang, S.; Schröder, M.; Nenoff, T.M. Reversible MOF-Based Sensors for the Electrical Detection of Iodine Gas. *ACS Appl. Mater. Interfaces* **2019**, *11*, 27982–27988. [CrossRef] [PubMed]
16. Cavallo, G.; Metrangolo, P.; Milani, R.; Pilati, T.; Priimagi, A.; Resnati, G.; Terraneo, G. The Halogen Bond. *Chem. Rev.* **2016**, *116*, 2478–2601. [CrossRef]
17. Cavallo, G.; Metrangolo, P.; Pilati, T.; Resnati, G.; Sansotera, M.; Terraneo, G. Halogen bonding: A general route in anion recognition and coordination. *Chem. Soc. Rev.* **2010**, *39*, 3772–3783. [CrossRef]
18. Dabranskaya, U.; Ivanov, D.M.; Novikov, A.S.; Matveychuk, Y.V.; Bokach, N.A.; Kukushkin, V.Y. Metal-Involving Bifurcated Halogen Bonding C–Br$\cdots\eta^2$ (Cl–Pt). *Cryst. Growth Des.* **2019**, *19*, 1364–1376. [CrossRef]
19. Eliseeva, A.A.; Ivanov, D.M.; Novikov, A.S.; Rozhkov, A.V.; Kornyakov, I.V.; Dubovtsev, A.Y.; Kukushkin, V.Y. Hexaiododiplatinate(ii) as a useful supramolecular synthon for halogen bond involving crystal engineering. *Dalton Trans.* **2020**, *49*, 356–367. [CrossRef]
20. Kinzhalov, M.A.; Kashina, M.V.; Mikherdov, A.S.; Mozheeva, E.A.; Novikov, A.S.; Smirnov, A.S.; Ivanov, D.M.; Kryukova, M.A.; Ivanov, A.Y.; Smirnov, S.N.; et al. Dramatically Enhanced Solubility of Halide-Containing Organometallic Species in Diiodomethane: The Role of Solvent$\cdots$Complex Halogen Bonding. *Angew. Chem. Int. Ed.* **2018**, *57*, 12785–12789. [CrossRef]
21. Awwadi, F.F.; Taher, D.; Haddad, S.F.; Turnbull, M.M. Competition between Hydrogen and Halogen Bonding Interactions: Theoretical and Crystallographic Studies. *Cryst. Growth Des.* **2014**, *14*, 1961–1971. [CrossRef]
22. Awwadi, F.F.; Haddad, S.F.; Turnbull, M.M.; Landee, C.P.; Willett, R.D. Copper–halide bonds as magnetic tunnels; structural, magnetic and theoretical studies of trans-bis(2,5-dibromopyridine)dihalo copper(ii) and trans-bis(2-bromopyridine)dibromo copper(ii). *CrystEngComm* **2013**, *15*, 3111–3118. [CrossRef]
23. Kalaj, M.; Momeni, M.R.; Bentz, K.C.; Barcus, K.S.; Palomba, J.M.; Paesani, F.; Cohen, S.M. Halogen bonding in UiO-66 frameworks promotes superior chemical warfare agent simulant degradation. *Chem. Commun.* **2019**, *55*, 3481–3484. [CrossRef] [PubMed]
24. Bertani, R.; Sgarbossa, P.; Venzo, A.; Lelj, F.; Amati, M.; Resnati, G.; Pilati, T.; Metrangolo, P.; Terraneo, G. Halogen bonding in metal–organic–supramolecular networks. *Coord. Chem. Rev.* **2010**, *254*, 677–695. [CrossRef]
25. Chernysheva, M.V.; Bulatova, M.; Ding, X.; Haukka, M. Influence of Substituents in the Aromatic Ring on the Strength of Halogen Bonding in Iodobenzene Derivatives. *Cryst. Growth Des.* **2020**, *20*, 7197–7210. [CrossRef]

26. Zaguzin, A.S.; Sukhikh, T.S.; Kolesov, B.A.; Sokolov, M.N.; Fedin, V.P.; Adonin, S.A. Iodinated vs non-iodinated: Comparison of sorption selectivity by $[Zn_2(bdc)_2dabco]_n$ and superstructural 2-iodoterephtalate-based metal–organic framework. *Polyhedron* **2022**, *212*, 115587. [CrossRef]
27. Perry, R.J.; Wilson, B.D.; Turner, S.R.; Blevins, R.W. Synthesis of Polyimides via the Palladium-Catalyzed Carbonylation of Bis(o-iodo esters) and Diamines. *Macromolecules* **1995**, *28*, 3509–3515. [CrossRef]
28. Sheldrick, G.M. SHELXT—Integrated space-group and crystal-structure determination. *Acta Crystallogr. Sect. A Found. Adv.* **2015**, *71*, 3–8. [CrossRef]
29. Sheldrick, G.M. Crystal structure refinement with SHELXL. *Acta Crystallogr. Sect. C Struct. Chem.* **2015**, *71*, 3–8. [CrossRef]
30. Hübschle, C.B.; Sheldrick, G.M.; Dittrich, B. ShelXle: A Qt graphical user interface for SHELXL. *J. Appl. Crystallogr.* **2011**, *44*, 1281–1284. [CrossRef]
31. Rubtsova, I.K.; Melnikov, S.N.; Shmelev, M.A.; Nikolaevskii, S.A.; Yakushev, I.A.; Voronina, J.K.; Barabanova, E.D.; Kiskin, M.A.; Sidorov, A.A.; Eremenko, I.L. Facile synthesis and structure elucidation of metal-organic frameworks with {ZnCa} and $\{Zn_2Ca\}$ metal cores. *Mendeleev Commun.* **2020**, *30*, 722–724. [CrossRef]
32. Nikiforova, M.E.; Lutsenko, I.A.; Kiskin, M.A.; Nelyubina, Y.V.; Primakov, P.V.; Bekker, O.B.; Khoroshilov, A.V.; Eremenko, I.L. Coordination Polymer of Ba^{2+} with 2-Furoic Acid Anions: Synthesis, Structure, and Thermal Properties. *Russ. J. Inorg. Chem.* **2021**, *66*, 1343–1349. [CrossRef]
33. Dubskikh, V.A.; Lysova, A.A.; Samsonenko, D.G.; Dybtsev, D.N.; Fedin, V.P. Synthesis and structures of coordination polymers based on a bridging ligand with the thienothiophene backbone. *J. Struct. Chem.* **2022**, *63*, 227–234. [CrossRef]
34. Dong, Y.J.; Fu, W.W.; Gui, S.Y.; Liu, X.; Zi, L.L.; Wang, L.S. Syntheses, Crystal Structures, and Magnetic Properties of Two Cobalt(II) Coordination Complexes with 4′-Substituted 3,2′:6′,3″-Terpyridine Ligands. *Russ. J. Coord. Chem.* **2022**, *48*, 659–666. [CrossRef]
35. Burlak, P.V.; Kovalenko, K.A.; Samsonenko, D.G.; Fedin, V.P. Cadmium(II)-Organic Frameworks Containing the 1,3-Bis(2-methylimidazolyl)propane Ligand. *Russ. J. Coord. Chem.* **2022**, *48*, 504–509. [CrossRef]
36. Demakov, P.A.; Fedin, V.P. Layered trans-1,4-Cyclohexanedicarboxylates of Divalent Metals: Synthesis, Crystal Structures, and Thermal Properties. *Russ. J. Coord. Chem.* **2022**, *48*, 270–277. [CrossRef]
37. Kalyakina, A.S.; Utochnikova, V.V.; Zimmer, M.; Dietrich, F.; Kaczmarek, A.M.; Van Deun, R.; Vashchenko, A.A.; Goloveshkin, A.S.; Nieger, M.; Gerhards, M.; et al. Remarkable high efficiency of red emitters using Eu(iii) ternary complexes. *Chem. Commun.* **2018**, *54*, 5221–5224. [CrossRef]
38. Utochnikova, V.V.; Kuzmina, N.P. Photoluminescence of lanthanide aromatic carboxylates. *Russ. J. Coord. Chem.* **2016**, *42*, 679–694. [CrossRef]
39. Utochnikova, V.V.; Abramovich, M.S.; Latipov, E.V.; Dalinger, A.I.; Goloveshkin, A.S.; Vashchenko, A.A.; Kalyakina, A.S.; Vatsadze, S.Z.; Schepers, U.; Bräse, S.; et al. Brightly luminescent lanthanide pyrazolecarboxylates: Synthesis, luminescent properties and influence of ligand isomerism. *J. Lumin.* **2019**, *205*, 429–439. [CrossRef]
40. Utochnikova, V.V.; Grishko, A.; Vashchenko, A.; Goloveshkin, A.; Averin, A.; Kuzmina, N. Lanthanide Tetrafluoroterephthalates for Luminescent Ink-Jet Printing. *Eur. J. Inorg. Chem.* **2017**, *2017*, 5635–5639. [CrossRef]
41. Kalyakina, A.S.; Utochnikova, V.V.; Bushmarinov, I.S.; Ananyev, I.V.; Eremenko, I.L.; Volz, D.; Rönicke, F.; Schepers, U.; Van Deun, R.; Trigub, A.L.; et al. Highly Luminescent, Water-Soluble Lanthanide Fluorobenzoates: Syntheses, Structures and Photophysics, Part I: Lanthanide Pentafluorobenzoates. *Chem. Eur. J.* **2015**, *21*, 17921–17932. [CrossRef] [PubMed]
42. Utochnikova, V.V.; Kotova, O.V.; Shchukina, E.M.; Eliseeva, S.V.; Kuz'mina, N.P. Gas-phase synthesis of terbium and lutetium carboxylates. *Russ. J. Inorg. Chem.* **2008**, *53*, 1878–1884. [CrossRef]
43. Bünzli, J.-C.G.; Piguet, C. Taking advantage of luminescent lanthanide ions. *Chem. Soc. Rev.* **2005**, *34*, 1048–1077. [CrossRef] [PubMed]
44. De Oliveira, G.M.; MacHado, A.; Gomes, G.W.; Monteiro, J.H.S.K.; Davolos, M.R.; Abram, U.; Jagst, A. Integrated X-ray crystallography, optical and computational methods in studies of structure and luminescence of new synthesized complexes of lanthanides with ligands derived from 2,6-diformylpyridine. *Polyhedron* **2011**, *30*, 851–859. [CrossRef]